Stepping rotation of F_1-ATPase visualized through angle-resolved single-fluorophore imaging

Kengo Adachi*[†], Ryohei Yasuda[†], Hiroyuki Noji[†], Hiroyasu Itoh[†‡], Yoshie Harada[†§], Masasuke Yoshida[†¶], and Kazuhiko Kinosita, Jr.[†§||]

*Department of Physics, Faculty of Science, Kanazawa University, Kakuma-machi, Kanazawa 920-1192, Japan; [†]Core Research for Evolutional Science and Technology, ''Genetic Programming'' Team 13, Nogawa, Miyamae-ku, Kawasaki 216-0001, Japan; [‡]Tsukuba Research Laboratory, Hamamatsu Photonics K. K., Tsukuba 300-2635, Japan; [¶]Research Laboratory of Resources Utilization, Tokyo Institute of Technology, Midori-ku, Yokohama 226-8503, Japan; and [§]Department of Physics, Faculty of Science and Technology, Keio University, Kohoku-ku, Yokohama 223-8522, Japan

Orientation dependence of single-fluorophore intensity was exploited in order to videotape conformational changes in a protein machine in real time. The fluorophore Cy3 attached to the central subunit of F_1-ATPase revealed that the subunit rotates in the molecule in discrete 120° steps and that each step is driven by the hydrolysis of one ATP molecule. These results, unlike those from the previous study under a frictional load, show that the 120° stepping is a genuine property of this molecular motor. The data also show that the rate of ATP binding is insensitive to the load exerted on the rotor subunit.

Conformational changes in protein molecules during function are best studied at the single-molecule level, because the operation of protein machines is always stochastic and thus such operations cannot be synchronized with each other. Individual behaviors can be assessed by single-fluorophore imaging (1–5), which is much less perturbing than imaging through a huge tag such as a plastic bead or actin filament (6). Real-time determination of fluorophore orientation (5, 7, 8) should be particularly useful, because a conformational change necessarily accompanies reorientation of one part against others. Thus far, however, successful applications of this potentially powerful method have been made infrequently. Herein, we show reorientation of a subunit in F_1-ATPase by using angle-resolved single-fluorophore imaging.

The F_1-ATPase is a part of ATP synthase that couples proton flow through its F_o portion to synthesis/hydrolysis of ATP in F_1 (9). Isolated F_1 consisting of $\alpha_3\beta_3\gamma_1\delta_1\varepsilon_1$-subunits only hydrolyzes ATP and is called F_1-ATPase. In a crystal structure of F_1 (10), the γ-subunit is surrounded by a cylinder made of alternating α- and β-subunits. Rotation of γ within the $\alpha_3\beta_3$-hexamer has been suggested (11–13) and confirmed (14–20). In our previous studies (18, 20), the rotation was visualized under a microscope by attaching an actin filament to γ. The filament rotated counterclockwise when viewed from the F_o side and in discrete 120° steps as predicted from the presence of three catalytic sites, one each on β (10). The long actin filament, however, may have altered the genuine kinetics of the F_1 motor, because the filament was subject to a large hydrodynamic friction. Also, the 120° stepping could have resulted from frictional obstruction of the filament motion by the $\alpha_3\beta_3$-hexamer with pseudo-3-fold symmetry. Measurement of rotation with a much smaller probe is desired. Thus, we examined rotational characteristics of F_1 with no load by attaching a single fluorophore to γ and assessing the fluorophore orientation through its polarized fluorescence on a microscope with an extremely low background (4, 21).

Materials and Methods

Protein Preparation. The subcomplex $\alpha(C193S)_3\beta(His_{10}$-tag at N terminus)$_3\gamma(I210C)$ derived from thermophilic *Bacillus* PS3 was mixed with a 1.1-fold molar excess of Cy3-maleimide (Amersham Pharmacia) in 20 mM Mops-KOH (pH 7.0) and 100 mM KCl for 30 min at room temperature. Unreacted Cy3-maleimide was removed on a Superdex 200 column (Amersham Pharmacia) to terminate the reaction. The labeling ratio was determined to be 0.75 mol Cy3 per mol F_1, by assuming $\varepsilon_{555}^{Cy3} = 150,000$ $M^{-1}\cdot cm^{-1}$ (22), $\varepsilon_{280}^{Cy3} = 15,000\ M^{-1}\cdot cm^{-1}$, and $\varepsilon_{280}^{F1} = 154,000$ $M^{-1}\cdot cm^{-1}$ (23).

Ni^{2+}-Nitrilotriacetic Acid (Ni-NTA) Surface. Glass coverslips (Micro-Cover Glass, No. 1, $24 \times 36\ mm^2$, Matsunami, Japan) precleaned with KOH were immersed in 0.01% acetic acid containing 2% (vol/vol) 3-glycidyloxypropyl-trimethoxysilane (Fluka) for 3 h at 90°C and washed with water. The glass was incubated in 0.01 M $NaHCO_3$ (pH 10.0) containing 10% (wt/vol) N-(5-amino-1-carboxypentyl)-iminodiacetic acid (Qiagen, Hilden, Germany) for 16 h at 60°C and washed with water. Then, the glass was incubated in 10 mM $NiCl_2$ (or $NiSO_4$) and 5 mM glycine (pH 8.0) for 2 h at room temperature, washed with water, and stored in water until use.

Rotation Assay. A flow chamber (18) was constructed of a bottom coverslip ($24 \times 36\ mm^2$) coated with Ni-NTA and an uncoated top coverslip ($18 \times 18\ mm^2$), and 50 pM Cy3-$\alpha_3\beta_3\gamma$ in buffer A (50 mM KCl/4 mM $MgCl_2$/10 mM Mops-KOH, pH 7.0) was infused. After 2 min, the chamber was washed with five volumes of buffer A and then with five volumes of degassed buffer A containing 0.5% 2-mercaptoethanol, 216 μg/ml glucose oxidase, 360 μg/ml catalase, 4.5 mg/ml glucose, 0.2 mg/ml creatine kinase, 2.5 mM creatine phosphate, and the desired amount of ATP. Washing with buffer A plus 500 mM imidazole removed ≈80% of fluorescent spots, whereas buffer A plus 500 mM KCl removed ≈10%, and <3% of spots were observed with unlabeled F_1.

ATPase Activity. F_1 was passed through a Butyl-Toyopearl column (Tosoh, Tokyo) equilibrated with 10% (vol/vol) $(NH_4)_2SO_4$/2 mM EDTA/100 mM potassium phosphate, pH 7.0 to reduce the bound nucleotide to ≈0.05 mol per mol F_1 as confirmed with reverse-phase HPLC (ODS-80Ts, Tosoh). ATPase activity was determined at 23°C with an ATP-regenerating system (24) containing 1 mM phosphoenolpyruvate, 200 μg/ml pyruvate kinase, 100 μg/ml lactate dehydrogenase, 0.15 mM NADH, and indicated ATP in buffer A. The initial hydrolysis rate was determined from the slope of absorbance decrease at 340 nm, allowing for the mixing time of 1.5 s.
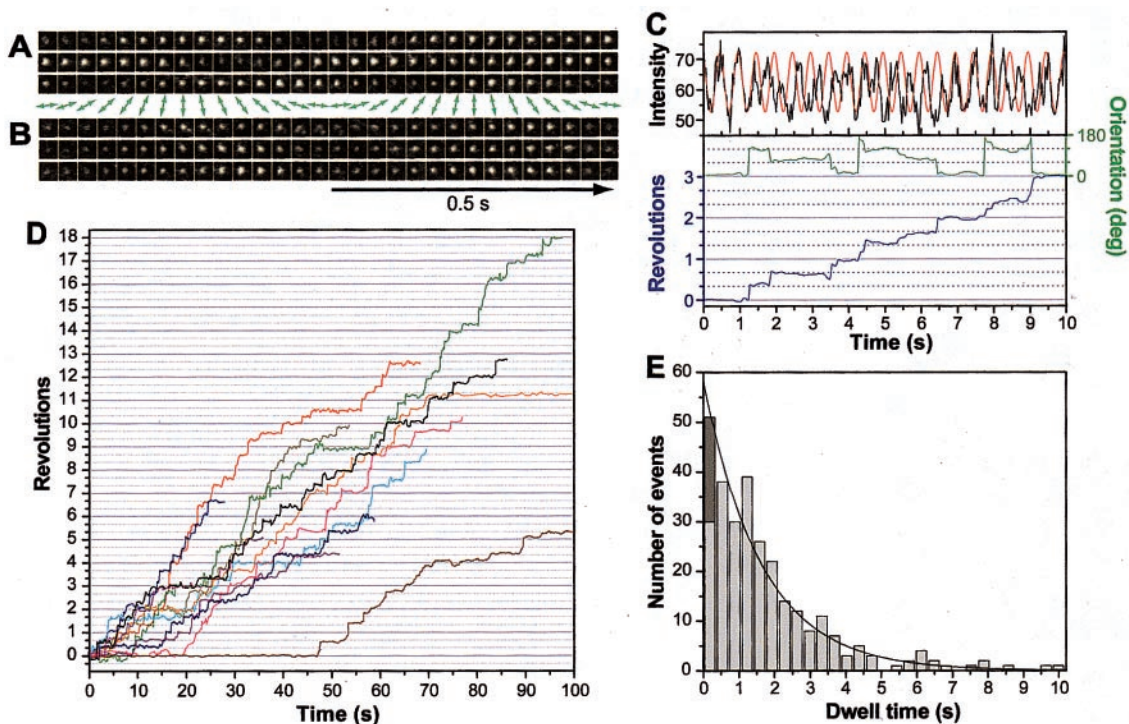

Fig. 1. (*A* and *B*) Sequential fluorescence images, at 33-ms intervals, of single Cy3-F$_1$ molecules at 20 nM ATP. The direction of excitation polarization is shown in green arrows. Each image was averaged spatially over 3 × 3 pixels (0.30 × 0.30 μm^2); the size of images shown is 17 × 17 pixels. The excitation intensity was 1.1 mW over a sample area of 24 μm in diameter. (*C*) Time courses of the fluorescence intensity and calculated fluorophore angles. The black line shows the intensity at time *t*, *I*(*t*), of the spot in *A* integrated over a square of 0.79 × 0.79 μm^2 enclosing the spot. When a fluorophore lies at an angle θ in the sample plane, its intensity is expected to flicker as $\cos^2[360°\cdot(t/T) - \theta] \propto \cos[360°\cdot(2t/T) - 2\theta]$, where *T* (1 s) is the period of excitation rotation. Thus, $\theta(t)$ was determined by fitting the observed *I*(*t*) with this function over the period between *t* and *t* + *T*/2. The green curve shows $\theta(t) - \theta_0$, where $\theta_0 = \theta(0)$; values between 0° and 180° were chosen. If this fluorophore had remained at θ_0, *I*(*t*) would have flickered as in the red line which is proportional to $\cos^2[360°\cdot(t/T) - \theta_0] \propto \cos[360°\cdot(2t/T) - 2\theta_0]$. The accumulated rotation angle (blue line) was obtained by assuming that all steps were counterclockwise. (*D*) Time courses of the stepwise rotation of the γ-subunit at 20 nM ATP. Different lines show different fluorophores (F$_1$). (*E*) Distribution of dwell times between steps. Each negative 120° step in the orientation records was interpreted as a zero dwell between two consecutive counterclockwise steps and counted as one in the dark part. The solid line shows the exponential fit. The average dwell time was 2.0 s.

ATPase activity of F$_1$ attached on the Ni-NTA glass surface was measured with a Malachite Green Pi assay (25, 26); 15 μl of 0.5 nM Cy3-$\alpha_3\beta_3\gamma$ in buffer A was infused into a chamber with both top and bottom coverslips coated with Ni-NTA. After 2 min, the chamber was washed with 200 μl of buffer A. ATPase reaction was started by infusing buffer A containing 2 mM ATP. After an incubation time of 10–55 min, 50 μl of buffer A was added from one edge of the chamber, and the solution containing liberated Pi was collected from the other edge. This procedure was repeated five times, and 200 μl of the collected solution was mixed with 500 μl of a Malachite Green reagent (Iatron Laboratories, Tokyo). After 10 s, 75 μl of 34% (wt/vol) sodium-citrate was added. After 12 min, the absorbance at 650 nm was measured. In control experiments without F$_1$, the absorbance was independent of the incubation time. The absorbance for samples with F$_1$, after subtraction of the control value, was approximately proportional to the ATPase reaction times (10, 25, 40, and 55 min), indicating that a steady state was reached by 10 min. The number of subcomplex molecules in the chamber was estimated from the fluorescence intensity of Cy3.

Fluorescence Microscopy. A 532-nm laser beam (DPSS 532–200, Coherent, Tokyo) was circularly polarized with a quarter-wave plate and introduced into a fluorescence microscope (IX70, Olympus, Tokyo) through a side port as described in ref. 4. To rotate the excitation polarization, a rotating sheet polarizer was inserted after the quarter-wave plate. Fluorescence was collected through an oil-immersion objective (PlanApo 100×, NA 1.4,

Olympus) onto an intensified (VS4–1845, Videoscope, Sterling, VA) charge-coupled device camera (CCD-300T-IFG, Dage–MTI, Michigan City, IN). Observations were made at 23 ± 1°C. Images were recorded on a Hi8 video recorder (EVO-9650, Sony, Tokyo) and analyzed with a digital image processor (C2000, Hamamatsu Photonics, Hamamatsu City, Japan) and a personal computer.

Results and Discussion

To detect the rotation of the γ-subunit, the fluorophore should be firmly attached to γ. We thus tested several combinations of a γ-mutant (S107C, I210C, or S107C/I210C) and a fluorescent dye suitable for single-fluorophore imaging (tetramethylrhodamine-5-maleimide, Molecular Probes; Cy3-maleimide or Cy3-bis-maleimide, Amersham Pharmacia). Among these, a suspension of the subcomplex $\alpha_3\beta_3\gamma$(I210C), hereafter referred to as F$_1$, labeled with Cy3-maleimide at the sole cysteine in γ gave the highest fluorescence anisotropy of 0.32 [λ_{ex} = 550 nm; λ_{em} = 590 nm; measured in a Hitachi (Tokyo) F-4500 spectrofluorometer], indicating that the fluorophore wobble on this subcomplex was within a cone of semiangle <25°. This Cy3-labeled F$_1$ was fixed on a glass surface coated with Ni-NTA through histidines engineered in β such that the F$_o$ side would be away from the glass. Single Cy3 fluorophores were observed on the inverted epifluorescence microscope. The orientations of individual fluorophores, and thus of γ, were assessed by two methods: (*i*) from the polarization dependence of the efficiency of light ab-

Adachi *et al*.

sorption (7) and (ii) from the polarization of emitted fluorescence (5).

For method *i*, the polarization axis of excitation light was rotated continuously in the sample plane at 1 Hz, in the counterclockwise direction when viewed from the F_o side. Under these conditions, fluorophores are expected to fluoresce when the excitation polarization becomes parallel with their absorption transition moment. The fluorophore in Fig. 1*A* was initially at a vertical orientation, turned into an 8 o'clock–2 o'clock orientation in the second row, and then turned through 4 o'clock–10 o'clock to the vertical orientation. The fluorophore in Fig. 1*B*, in contrast, remained vertical, presumably being on an inactive F_1.** From the spot in Fig. 1*A*, we calculated the fluorophore orientation as in Fig. 1*C* (see legend for method). The orientation (green), determined within the cyclic redundancy of 180°, stepped among three levels. Because rotation was always counterclockwise in previous studies (18, 20), we interpret all steps as counterclockwise and show the resultant rotation angle in blue; negative 60° steps in green were interpreted as counterclockwise 120° steps. The negative 120° step at ≈9 s in green was interpreted as rapid succession of two counterclockwise 120° steps within the 0.5-s window used for the angle analysis. Stepping records at 20 nM ATP are summarized in Fig. 1*D*.

Fig. 1*E* shows a histogram of the dwell times between steps. Zero dwells between rapid succession of two steps, converted from negative 120° steps above, are distinguished in dark gray, because some of these may represent genuine backward (clockwise 120°) steps. If steps are all driven by one ATP molecule, the histogram should be an exponential function at low ATP concentrations ($<\mu M$) where ATP binding is rate limiting: $\exp(-k_{on}[ATP]t)$, where k_{on} is the rate constant for ATP binding and t is the dwell time. The experimental histogram, including the dark part, was indeed exponential with k_{on} of $3.1 \times 10^7 \, M^{-1}\cdot s^{-1}$, a value that agrees with the previous estimate with actin of $2 \times 10^7 \, M^{-1}\cdot s^{-1}$ to $3 \times 10^7 \, M^{-1}\cdot s^{-1}$ (20). Most of the steps counted in the dark bar are thus likely not backward steps. Genuine backward steps were observed with actin (20), but their frequency was at most a few percent.

In method *ii*, fluorescence was excited with circularly polarized light. The emission was decomposed into vertically (*V*) and horizontally (*H*) polarized components in a dual-view apparatus, and the two were simultaneously projected onto the video camera (5, 27). A vertically oriented fluorophore would show up in the *V* image, and a horizontal one would appear in *H*. Alternate appearance, as shown in Fig. 2*A*, indicates rotation of the γ-subunit. From the intensity records (Fig. 2*B*), polarization ($[V - H]/[V + H]$) was calculated (Fig. 2*C*) and showed three levels, a, b, and c. These levels can be explained by three orientations separated by 120° (Fig. 2*D*), again indicating stepping rotation.

**Approximately 70% of observed spots were unpolarized both in methods *i* and *ii*, presumably because of imperfect binding to the glass surface (rapid tumbling or wrong orientations of F_1 can result in unpolarized fluorescence). Of the polarized ≈30%, most were inactive, showing no time-dependent change in polarization direction. For *i* and *ii*, we analyzed 59,149 spots and selected for further analysis 76 spots that made three or more revolutions before photobleaching. When an actin filament was used as a marker of rotation (18, 20), the probability of finding a rotating filament was also low, at most a few percent and much less at low ATP concentrations. The reasons for the low yields are not clear but likely include surface denaturation and MgADP inhibition. The steady-state ATPase activity, at 2 mM ATP, of Cy3-F_1 attached to the Ni-NTA glass surface was 19 s^{-1} and was ≈30% of that in solution, suggesting that ≈70% was denatured on the surface. The initial activity in solution at 2 mM ATP was 239 s^{-1}, which decreased to the steady-state level of 67 s^{-1} because of the MgADP inhibition (28). These numbers imply that <10% of the F_1 molecules on the surface are expected to be active. Most of the active ones might have been in the unpolarized, imperfectly bound population, because binding through three histidine tags tethered at widely separated positions could potentially impose strain. The actual causes are yet to be determined.
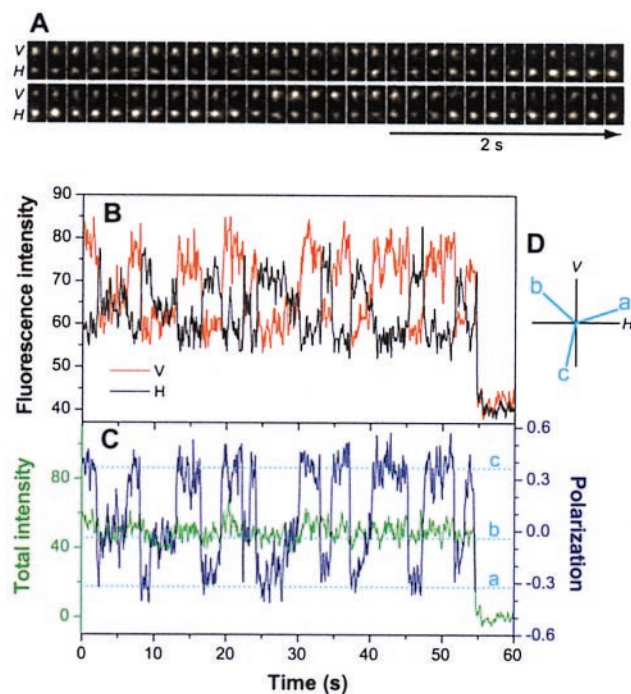

Fig. 2. (*A*) Sequential fluorescence images, at 167-ms intervals, of a single Cy3-F_1 molecule at 20 nM ATP. *V*, vertically polarized fluorescence; *H*, horizontally polarized fluorescence. Each image (15 × 30 pixels or 1.5 × 3.0 μm²) was averaged spatially over 3 × 3 pixels. (*B*) Time courses of spot intensities for *V* and *H* in *A*, median-filtered over eight video frames (0.27 s). (*C*) Time courses of the polarization, $P = (V - H)/(V + H)$, and total intensity, $I = V + H$, calculated from *B*. The fluorophore photobleached at ≈55 s. Dashed lines (a, b, and c) are calculated P for the three orientations in *D*: $P = 0.4 \times [\sin^2(\theta + 18°) - \cos^2(\theta + 18°)]$, where $\theta = 0°$, 120°, and 240°.

The alternation of the spot intensity became faster at higher ATP concentrations, as expected for the ATP-dependent rotation (Fig. 3*A*). Because three levels of polarization were not always apparent in the noisy data, we analyzed the time intervals for a full turn (red lines in Fig. 3*A*). If a turn is comprised of three 120° steps and if each step is driven by one ATP molecule, then the time for a full turn, *t*, is expected to be distributed, at low ATP concentrations, as $t^2\exp(-k_{on}[ATP]t)$, where k_{on} is the rate constant for ATP binding. The experimental histograms (Fig. 3*B*) could be fitted with this function, indicating 120° stepping. k_{on} was $1.9 \times 10^7 \, M^{-1}\cdot s^{-1}$ at 200 nM ATP, $2.3 \times 10^7 \, M^{-1}\cdot s^{-1}$ at 60 nM ATP, and $2.9 \times 10^7 \, M^{-1}\cdot s^{-1}$ at 20 nM ATP. These values are consistent with the results of method *i* and previous estimates with actin. Slightly smaller values at higher ATP concentrations may be due to limited temporal resolution.

The average stepping rates, defined as the inverse of average stepping time, for individual F_1 are shown in Fig. 4. Rates from single-fluorophore imaging are somewhat higher than the estimates with actin (20), because long actin filaments occasionally made long pauses, presumably caused by surface obstruction, which increased the average stepping time without significantly affecting k_{on} estimated from the histogram analysis. Preliminary measurements with probes of intermediate sizes (submicrometer beads) also show higher rates consistent with the present estimates (R.Y., unpublished work). The stepping rates paralleled the rate of ATP hydrolysis measured in solution (Fig. 4), supporting the contention of one step per one ATP molecule. The hydrolysis rate was not as high, however, probably because of heterogeneity: a small fraction of F_1 in solution was probably inactive, whereas
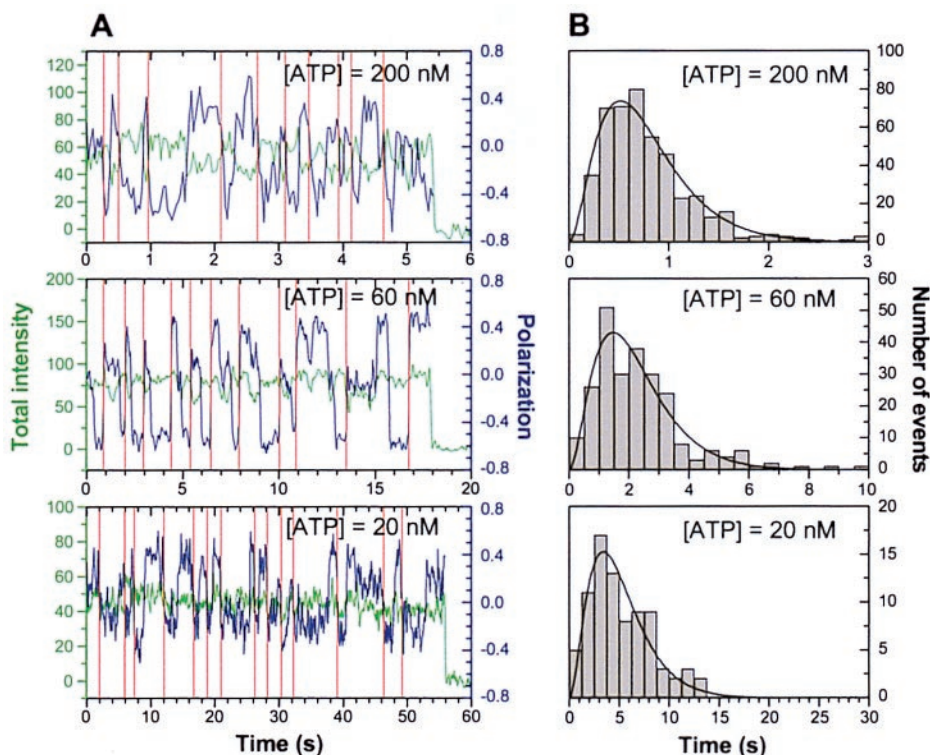
Fig. 3. (*A*) Alternation of polarization at various ATP concentrations. The excitation intensity was 6.2 mW at 200 nM ATP, 3.2 mW at 60 nM ATP, and 1.8 mW at 20 nM ATP over a sample area of 24 μm in diameter (the frequency of alternation did not depend on excitation intensity). The polarizations at 60 and 20 nM ATP were calculated after *V* and *H* were median-filtered over four and eight video frames, respectively. Vertical red lines indicate termination of one revolution, identified by eye as the crossing of polarization through zero in a unique direction. All records were terminated by photobleaching. (*B*) Distribution of times for a turn at various ATP concentrations. The average values were 0.84 s at 200 nM ATP, 2.4 s at 60 nM ATP, and 5.5 s at 20 nM ATP. Solid lines show fits with the equation in the text.
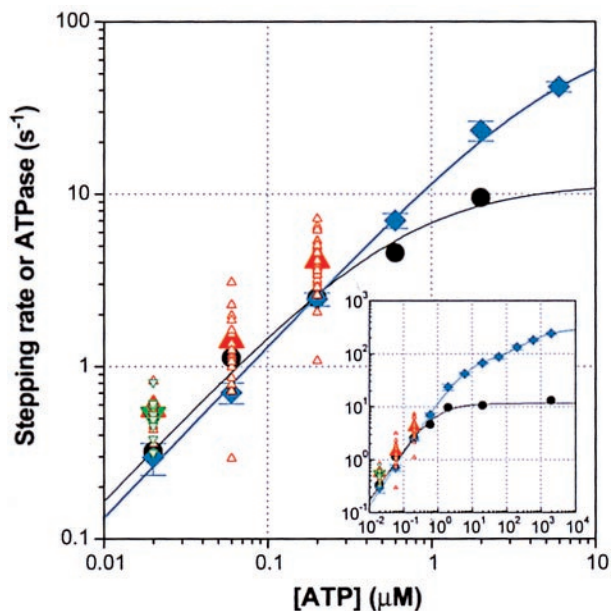

Fig. 4. Comparison of stepping and ATP hydrolysis rates. Stepping rate (3× rotation rate) was determined for each spot as 1/<*t*> or 3/<3*t*>, where <*t*> and <3*t*> are average times per step (*i*, green triangles) or turn (*ii*, red triangles), respectively. Larger symbols show averages over spots. Black circles show previous estimates with actin (20). Hydrolysis rate *V* (blue diamonds with error bars showing SD) was estimated in solution (i.e., the rate shown is the ensemble average over all molecules in the solution) and was fitted with $V = (k_{cat}^{a}K_{m}^{b}[ATP] + k_{cat}^{b}[ATP]^{2})/([ATP]^{2} + K_{m}^{b}[ATP] + K_{m}^{a}K_{m}^{b})$, where $k_{cat}^{a} = 83$ s^{-1}, $k_{cat}^{b} = 292$ s^{-1}, $K_{m}^{a} = 6.3$ μM, and $K_{m}^{b} = 680$ μM. Hydrolysis rate of Cy3-labeled F$_1$ (not shown) agreed within experimental error.

stepping rates were estimated on the most active F$_1$ in the sample. A likely cause is MgADP inhibition (28), which may also be responsible for the dip in hydrolysis rate around 10^1 to 10^2 μM ATP (Fig. 4 *Inset*). To estimate the hydrolysis rate in fully active samples, we carefully removed nucleotides from the F$_1$ preparation and measured the initial rate of hydrolysis. However, the possibility of rapid onset of MgADP inhibition during the initial period including the mixing time cannot be ignored.

In summary, by observing no-load rotation of F$_1$, we have shown that 120° stepping is a genuine characteristic of the F$_1$ motor, at least at low ATP concentrations and at the video-limited temporal resolution. Individual steps are powered by one ATP molecule. The kinetics of stepping or of ATP binding seem to be independent of the load. Because the rate of ATP binding likely depends on the orientation of γ (28–30), the rate could in principle vary depending on the load. At least for the frictional load on the actin filament, such variation does not seem to occur.

The polarization-analyzed single-fluorophore imaging should be useful in elucidating conformational changes in other protein (and RNA) machines as well. Method *i*, being superior in angular resolution, and method *ii*, having theoretically unlimited time resolution, are complementary.

1. Moerner, W. E. (1997) *Science* **277,** 1059–1060.
2. Ishikawa, M., Hirano, K., Hayakawa, T., Hosoi, S. & Brenner, S. (1994) *Jpn. J. Appl. Phys.* **33,** 1571–1576.
3. Funatsu, T., Harada, Y., Tokunaga, M., Saito, K. & Yanagida, T. (1995) *Nature (London)* **374,** 555–559.
4. Sase, I., Miyata, H., Corrie, J. E., Craik, J. S. & Kinosita, K., Jr. (1995) *Biophys. J.* **69,** 323–328.
5. Sase, I., Miyata, H., Ishiwata, S. & Kinosita, K., Jr. (1997) *Proc. Natl. Acad. Sci. USA* **94,** 5646–5650.
6. Kinosita, K., Jr. (1999) *FASEB J.* **13,** S201–S208.
7. Ha, T., Enderle, T., Chemla, D. S., Selvin, P. R. & Weiss, S. (1996) *Phys. Rev. Lett.* **77,** 3979–3982.
8. Warshaw, D. M., Hayes, E., Gaffney, D., Lauzon, A. M., Wu, J., Kennedy, G., Trybus, K., Lowey, S. & Berger, C. (1998) *Proc. Natl. Acad. Sci. USA* **95,** 8034–8039.
9. Boyer, P. D. (1997) *Annu. Rev. Biochem.* **66,** 717–749.
10. Abrahams, J. P., Leslie, A. G., Lutter, R. & Walker, J. E. (1994) *Nature (London)* **370,** 621–628.
11. Boyer, P. D. & Kohlbrenner, W. E. (1981) in *Energy Coupling in Photosynthesis*, eds. Selman, B. R. & Selman-Reimer, S. (Elsevier, Amsterdam), pp. 231–240.
12. Oosawa, F. & Hayashi, S. (1986) *Adv. Biophys.* **22,** 151–183.
13. Boyer, P. D. (1993) *Biochim. Biophys. Acta* **1140,** 215–250.
14. Duncan, T. M., Bulygin, V. V., Zhou, Y., Hutcheon, M. L. & Cross, R. L. (1995) *Proc. Natl. Acad. Sci. USA* **92,** 10964–10968.
15. Sabbert, D., Engelbrecht, S. & Junge, W. (1996) *Nature (London)* **381,** 623–625.
16. Zhou, Y., Duncan, T. M., Bulygin, V. V., Hutcheon, M. L. & Cross, R. L. (1996) *Biochim. Biophys. Acta* **1275,** 96–100.
17. Aggeler, R., Ogilvie, I. & Capaldi, R. A. (1997) *J. Biol. Chem.* **272,** 19621–19624.
18. Noji, H., Yasuda, R., Yoshida, M. & Kinosita, K., Jr. (1997) *Nature (London)* **386,** 299–302.
19. Häsler, K., Engelbrecht, S. & Junge, W. (1998) *FEBS Lett.* **426,** 301–304.
20. Yasuda, R., Noji, H., Kinosita, K., Jr., & Yoshida, M. (1998) *Cell* **93,** 1117–1124.
21. Adachi, K., Kinosita, K., Jr., & Ando, T. (1999) *J. Microsc. (Oxford)* **195,** 125–132.
22. Ernst, L. A., Gupta, R. K., Mujumdar, R. B. & Waggoner, A. S. (1989) *Cytometry* **10,** 3–10.
23. Matsui, T., Muneyuki, E., Honda, M., Allison, W. S., Dou, C. & Yoshida, M. (1997) *J. Biol. Chem.* **272,** 8215–8221.
24. Kato, Y., Sasayama, T., Muneyuki, E. & Yoshida, M. (1995) *Biochim. Biophys. Acta* **1231,** 275–281.
25. Ohno, T. & Kodama, T. (1991) *J. Physiol. (London)* **441,** 685–702.
26. Harada, Y., Sakurada, K., Aoki, T., Thomas, D. D. & Yanagida, T. (1990) *J. Mol. Biol.* **216,** 49–68.
27. Kinosita, K., Jr., Itoh, H., Ishiwata, S., Hirano, K., Nishizaka, T. & Hayakawa, T. (1991) *J. Cell. Biol.* **115,** 67–73.
28. Kinosita, K., Jr., Yasuda, R., Noji, H. & Adachi, K. (2000) *Philos. Trans. R. Soc. London B* **355,** 473–490.
29. Wang, H. & Oster, G. (1998) *Nature (London)* **396,** 279–282.
30. Kinosita, K., Jr., Yasuda, R. & Noji, H. (2000) *Essays Biochem.* **35,** in press.